Research Square

Preprints are preliminary reports that have not undergone peer review.
They should not be considered conclusive, used to inform clinical practice,
or referenced by the media as validated information.

Uremic toxin lanthionine interferes with VEGFA, intracellular calcium and PI3K/AKT/mTOR signaling pathway in A-498 clear cell renal carcinoma

Annapaola Coppola
University of Campania "Luigi Vanvitelli"
Patrizia Lombari
University of Campania "Luigi Vanvitelli"
Christian Di Maro
University of Campania "Luigi Vanvitelli"
Antonio D'Andrea
University of Campania "Luigi Vanvitelli"
Diana Ingrosso
University of Campania "Luigi Vanvitelli"
Giovanna Capolongo
University of Campania "Luigi Vanvitelli"
Mariadelina Simeoni
University of Campania "Luigi Vanvitelli"
Alessandra F. Perna
University of Campania "Luigi Vanvitelli"
Diego Ingrosso
University of Campania "Luigi Vanvitelli"
Margherita Borriello
margherita.borriello@unicampania.it

Pegaso University

Article

Keywords:

Posted Date: November 4th, 2026

DOI: https://doi.org/10.21203/rs.3.rs-11303119/v1

License: This work is licensed under a Creative Commons Attribution 4.0 International License.
Read Full License

Additional Declarations: No competing interests reported.

Uremic toxin lanthionine interferes with VEGFA, intracellular calcium and PI3K/AKT/mTOR signaling pathway in A-498 clear cell renal carcinoma

Annapaola Coppola[1†], Patrizia Lombari[1†], Christian Di Maro[1], Antonio D'Andrea[1], Diana Ingrosso[2], Giovanna Capolongo[3], Mariadelina Simeoni[3], Alessandra F. Perna[3], Diego Ingrosso[1] and Margherita Borriello[4*]

1. Department of Precision Medicine, University of Campania Luigi Vanvitelli, Naples, Italy
2. Department of Experimental Medicine, University of Campania, Luigi Vanvitelli, Naples, Italy.
3. Department of Translational Medical Science, University of Campania Luigi Vanvitelli, Naples, Italy
4. Department of Psychology and Health Science, Pegaso University, Naples, Italy.

†These authors equally contributed to this work

*Corresponding author: margherita.borriello@unicampania.it

Abstract

Chronic kidney disease (CKD) and cancer are major and increasingly interconnected health burdens. Uremic toxins, which accumulate as kidney function declines, have been implicated in cancer progression, including site-specific renal cell carcinoma (RCC), but the molecular mechanisms underlying these effects remain poorly understood.

This study investigated the effect of lanthionine, a sulfur-containing uremic toxin detected in CKD, at clinically relevant concentrations, in A-498 cells as human clear cell renal carcinoma cell line (ccRCC), and HEK293 as non-malignant renal cells.

Our results showed that lanthionine acts in a cell-specific manner, promoting cancer cell migration and invasion, with a more pronounced effect in A-498 cells. Lanthionine selectively modulated VEGFA expression and protein levels in A-498 cells, promoting intracellular calcium levels and PI3K/AKT/mTOR signaling pathway. VEGFA increase appeared to be supported by HIFs overexpression. Importantly, VEGFA silencing in A-498 cells decreased intracellular calcium levels and inhibited PI3K/AKT/mTOR signaling pathway, supporting a functional link between VEGFA and these signaling events.

These results provide preliminary *in vitro* evidence that lanthionine may contribute to ccRCC progression by modulating VEGFA-associated calcium signaling and the PI3K/AKT/mTOR pathway, highlighting a potential molecular link between the uremic milieu and renal cancer progression.

Keywords: CKD, uremic toxin, lanthionine, renal cell carcinoma; VEGFA.

1. Introduction

Chronic kidney disease (CKD) is a growing health problem that affects 10% of the general population worldwide, and it is estimated that more than 850 million people will be affected in 2040 [1].
CKD results from a broad spectrum of conditions, including diabetes, hypertension, metabolic disorders, glomerular and genetic diseases, congenital anomalies of kidneys and urinary tract [2,3].
Progressive loss of renal function is accompanied by profound systemic alterations, including chronic inflammation, oxidative stress, disturbances in mineral and bone metabolism and the progressive accumulation of uremic toxins (UTs), promoting the transition to End Stage Renal Disease (ESRD), a condition strongly associated with elevated cardiovascular risk and mortality [4,5].
UTs are waste products that accumulate due to impaired kidney function and cannot be effectively eliminated [6]. Notably, even with regular dialysis treatment in ESRD, UTs are not fully cleared and continue circulating through the bloodstream, inducing several negative effects on various organs, especially on cardiovascular system [7].
UTs are well known for their cardiotoxic effects, contributing to endothelial dysfunction, vascular fibrosis, cardiac hypertrophy, oxidative stress, and inflammation, all of which are associated with an increased mortality risk [4,8–11].
Notably, several of these pathogenic mechanisms are shared by CKD and cancer.
The relationship between CKD and cancer has been investigated for more than five decades. Studies have reported an increased incidence of several malignancies among patients with impaired kidney function, especially during uremia, with cancers of the kidney and urinary tract among the most frequently observed [12,13].
In the case of renal cancer, its development has been clearly associated with traditional modifiable and fixed risk factors, such as obesity and hypertension [14]. By contrast, the role of non-traditional risk factors remains insufficiently defined and requires further elucidation [15].
Studies suggest that CKD may directly contribute to the development of renal cell carcinoma (RCC). This association is likely bidirectional: CKD may promote carcinogenesis through chronic inflammation, oxidative stress, metabolic alterations, acquired cystic kidney disease, and persistent exposure to uremic metabolites, whereas RCC may contribute to or accelerate CKD through nephrectomy, compensatory hyperfiltration, treatment-related kidney injury, and other mechanisms [16].
Clear cell renal cell carcinoma (ccRCC) accounts for approximately 70-80% of all diagnosed renal cancer cases [17]. This histotype is notably resistant to chemotherapy [18] and is characterized by metabolic gene alterations that drive the oncologic-metabolic underlying malignancy. In addition, ccRCC is characterized by frequent alterations in the von Hippel–Lindau (VHL) pathway. Loss of VHL function leads to stabilization of hypoxia-inducible factors (HIFs), which regulate the expression of several genes involved in angiogenesis, metabolism, proliferation, and tumor progression [19].
Beyond these mechanisms, accumulating evidence suggests that UTs are directly implicated in the progression of several solid tumors [20]. In particular, p-cresol, a major byproduct of tyrosine fermentation, causes dose and time-dependent effects on bladder cancer cells, promoting invasion and migration of living cells [21]. Moreover, it contributes to malignant biological behavior of HepG2 hepatocellular carcinoma cells [21]. Other studies highlighted the impact of indoxyl sulfate (IS) and p-cresyl sulfate (pCS), metabolites derived from intestinal tryptophan and tyrosine in the intestine. Specifically, IS has been demonstrated to promote colorectal cancer cell proliferation [22] and to enhance metastatic traits in ovarian cancer cells [23]. Conversely, pCS have been shown to induce proliferation and endothelial mesenchymal transition in ccRCC via the miR-21/HIF-1α signaling pathway [24].
Lanthionine, a sulfur containing UT with several untoward effects, is a natural non-proteogenic amino acid, generated as a side-product of the action of transsulfuration enzymes, *i.e.* cystathionine beta synthase (CBS) and cystathionine gamma-lyase (CSE), in hydrogen sulfide (H_2S) biosynthesis [11,25–30].

Interestingly, Hellmich and colleagues reported increased CBS expression in human colon cancer tissue and proposed urinary lanthionine as a potential biochemical marker of CBS upregulation, linking lanthionine metabolism to tumor-associated processes [31].
However, whether lanthionine directly affects renal cancer cells, and particularly the signaling pathways governing ccRCC progression remain unknown.
In this preliminary study, we investigated the effects of lanthionine, at concentration comparable to those detected in CKD patients [25,29,30], on ccRCC cell line A-498 and HEK293 cells, which served as non-cancerous renal controls.
By addressing these mechanisms, we aimed to determine whether lanthionine may represent a molecular link between the uremic milieu and the aggressive phenotype of ccRCC.

2. Results

2.1 Effect of lanthionine on cell migration and cell viability in A-498 and HEK293 cells

Images of cell cultures monitored until complete scratch closure (at 24 hours) are reported in Fig. 1a, b. Quantitative analysis of scratch area over time is presented on Fig. 1c, d.
In the A-498 cell line, treatments did not affect the wound closure at 6 hours, compared to control. After 9 hours, 0.3 µM lanthionine induced a closure comparable to the control, with a scratch area of 38%. At the same point, 1 µM lanthionine markedly enhanced closure, reducing the scratch area to approximately 20% (Figure1a, c).
In HEK293 cells, lanthionine at both concentrations did not significantly influence cell migration between 0 and 9 hours of treatment (Figure 1b, d).
Cell viability assessed with MTT assay revealed significant differences in A-498 cells, where both concentrations of lanthionine significantly increased viability at 48 hours. No effect was observed in HEK293 cell line (Supplementary Fig. S1a, b).

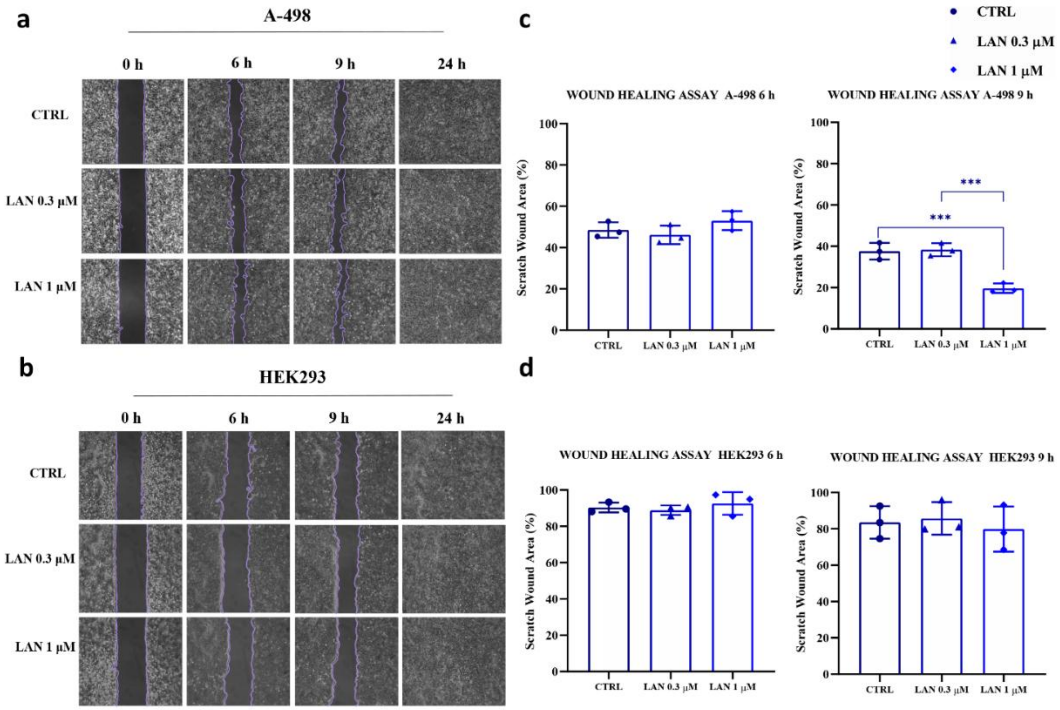


Figure 1. Wound healing assay in A-498 and HEK293 cell lines. (a, b) Images acquired of the scratch wound area at time 0, 6, 9 and 24 hours after treatment with 0.3 µM and 1 µM of lanthionine in A-498 and HEK293 cells. (c, d) Scratch wound area analysis, expressed as %, of A-498 and HEK293

cell lines. Histograms values are the mean ± standard deviation of three independent experiments: * $p \leq 0.05$, ** $p \leq 0.01$ and *** $p \leq 0.001$. CTRL: control; LAN 0.3 µM: lanthionine 0.3µM; LAN 1 µM: lanthionine 1 µM.

2.2 Effect of lanthionine on cell invasion in A-498 and HEK293 cells

Images of cell invasion ability after 20 hours of lanthionine treatment are shown in Fig. 2a, b. Quantitative analysis of cell invasion capacity, expressed as invasion index (%) after crystal violet staining, is reported in Fig. 2c, d. In A-498 cells, lanthionine induced a dose-dependent increase in cell invasion, resulting in an invasion index of 149.60% and 202.18% following treatment of 0.3 and 1 µM of lanthionine, respectively. In HEK293 cells, lanthionine at both concentrations did not significantly influence cell invasion after 20 hours of treatment (Fig. 2b, d), with a value of approximately 100%, comparable to the control.

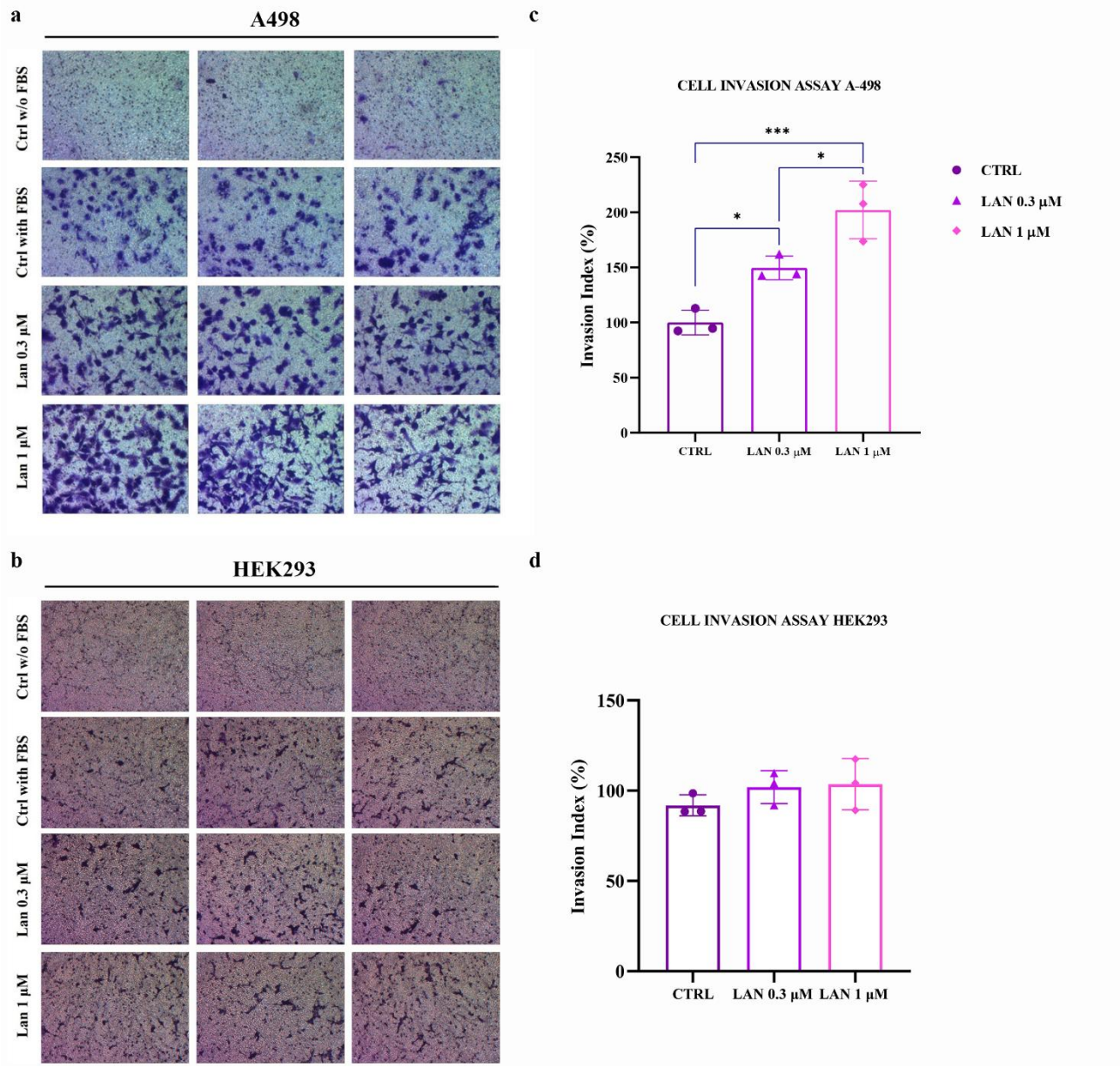


Figure 2. Transwell invasion assay in A-498 and HEK293 cell lines.
(a, b) Images acquired at 20 hours after treatment with 0.3 µM and 1 µM of lanthionine in A-498 and HEK293 cells. (c, d) Cell invasion analysis, expressed as invasion index (%), of A-498 and HEK293 cell lines. Histograms values are the mean ± standard deviation of three independent experiments: *

p ≤ 0.05, ** p ≤ 0.01 and *** p ≤ 0.001. CTRL w/o FBS: negative control without FBS. CTRL with FBS: positive control with FBS; LAN 0.3 µM: lanthionine 0.3µM; LAN 1 µM: lanthionine 1 µM.

2.3 Effect of lanthionine on intracellular calcium levels

Intracellular calcium levels detected after 30 minutes, 1, 2, 3 and 6 hours of treatment in A-498 and HEK293 cell lines are reported in Fig. 3 a, b. In A-498 cells, 0.3 µM lanthionine induced a significant increase in intracellular calcium levels after 30 minutes, 2 and 3 hours of treatments. At the same point, 1 µM of lanthionine led to a more significant increase in calcium levels, with a relevant effect even after 1 hour. No changes were detected at 6 hours of treatment (Figure 3a).
In HEK293 cells, lanthionine at both concentrations did not significantly influence calcium levels, as reported in Fig. 3b.

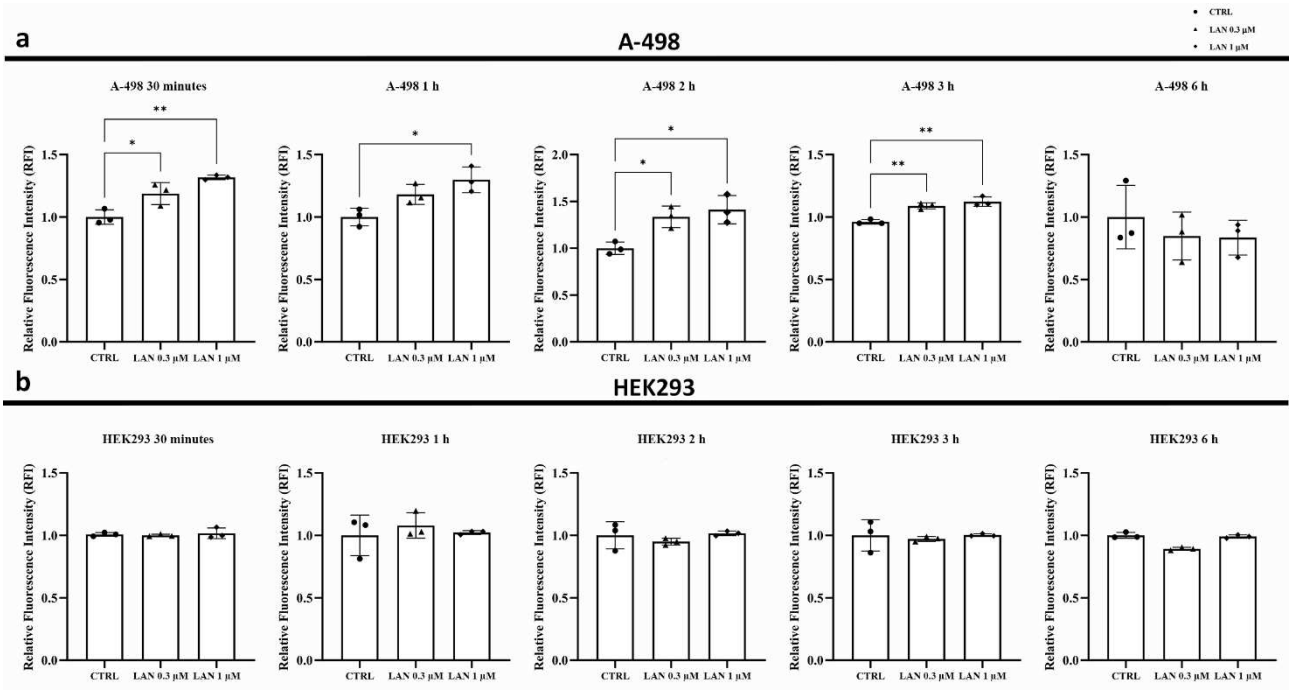


Figure 3. Intracellular calcium levels in A-498 and HEK293 cell lines.
(a) Results obtained in A-498 cells after 30 minutes, 1, 2, 3 and 6 hours of treatments with 0.3 µM and 1 µM of lanthionine. (b) Results obtained in HEK293 cells after 30 minutes, 1, 2, 3 and 6 hours of treatments with 0.3 µM and 1 µM of lanthionine. Results are expressed as relative fluorescence intensity (RFI). Histograms values are the mean ± standard deviation of three independent experiments: * p ≤ 0.05, ** p ≤ 0.01 and *** p ≤ 0.001. CTRL: control; LAN 0.3 µM: lanthionine 0.3µM: LAN 1 µM: lanthionine 1 µM.

2.4 Effect of lanthionine on VEGFA-PI3K/AKT/mTOR signal pathway in A-498 and HEK293 cells

VEGFA-PI3K/AKT/mTOR gene expression levels were analyzed after 24 and 48 hours of treatment. In A-498 cells, 1 µM of lanthionine increased VEGFA gene expression levels at both 24 and 48 hours of treatment (Fig. 4a, b). 1 µM of lanthionine raised PI3K expression after 24 hours of treatment, while an increase in AKT, mTOR, HIF2A and HIF1B has been detected at both 24 and 48 hours (Fig. 4a, b). While 0.3 µM of lanthionine was able to increase only the expression of HIF1B at 48 hours (Figure 4b).

In HEK293 cells, at 24 hours, a significant reduction of PI3K after 0.3 µM of lanthionine, of AKT after 1 µM of lanthionine and of mTOR after both treatments were detected (Figure 4c). At 48 hours, VEGFA, AKT and mTOR showed a significant reduction with 0.3 µM of lanthionine (Figure 4d). At the same time of treatment, 1 µM lanthionine induced only an increase in mTOR and HIF2A expression, while both concentrations were able to increase HIF1B gene levels compared to the control (Figure 4d).

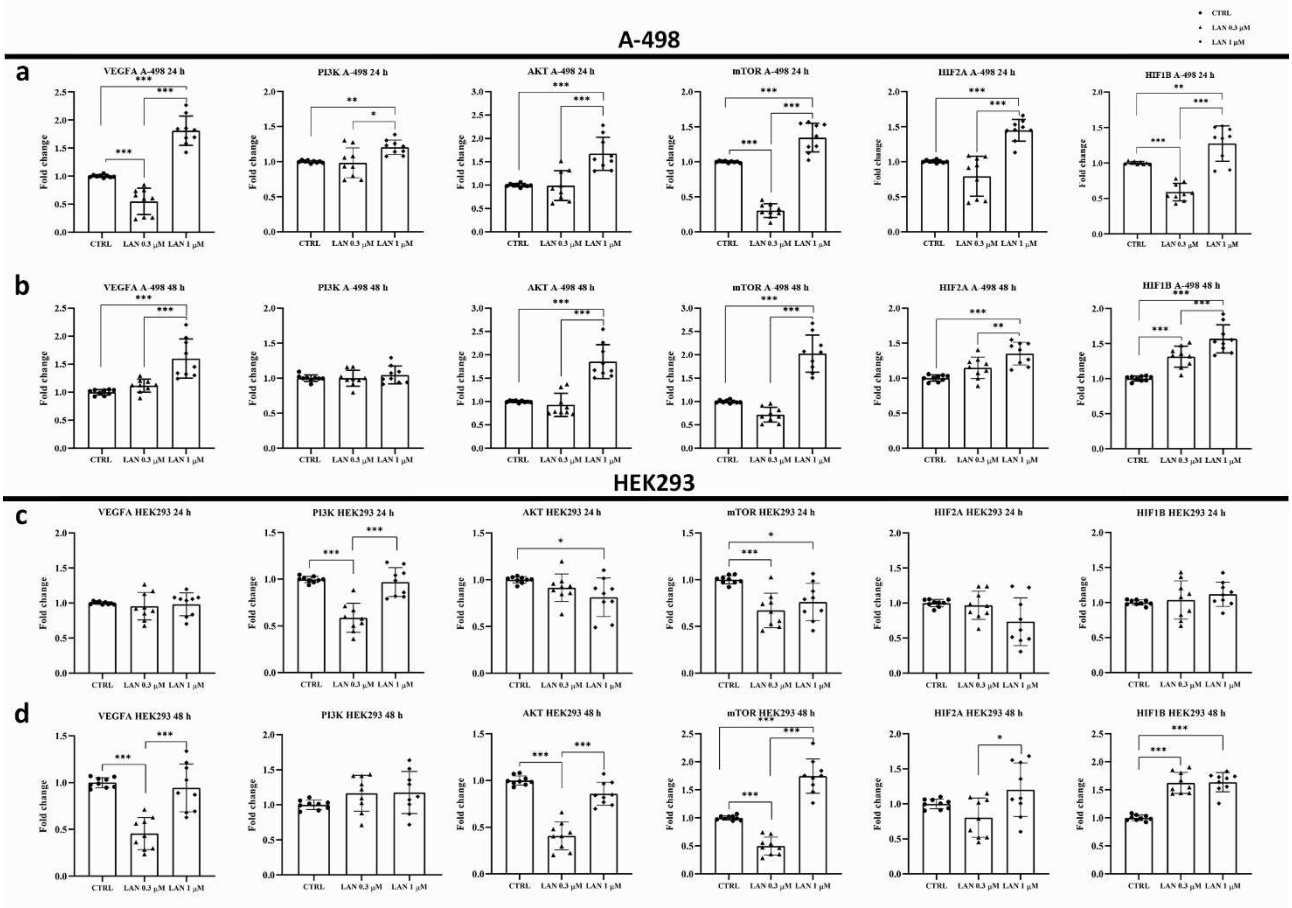


Figure 4. Real time PCR analysis of VEGFA, PI3K, AKT, mTOR, HIF2A and HIF1B after treatment with lanthionine in A-498 and HEK293 cell lines.

(a, b) Results obtained in A-498 cell line after 24 and 48 hours of treatment with lanthionine 0.3 µM and 1 µM. (c, d) Results obtained in HEK293 cell line after 24 and 48 hours of treatment with lanthionine 0.3 µM and 1 µM. Histograms values are the mean ± standard deviation of three independent experiments: * $p \leq 0.05$, ** $p \leq 0.01$ and *** $p \leq 0.001$. CTRL: control; LAN 0.3 µM: lanthionine 0.3µM: LAN 1 µM: lanthionine 1 µM.

2.5 Effect of lanthionine on VEGFA, PI3K, pAKT/AKT and pERK/ERK protein levels

In A-498 cells, 1 µM of lanthionine raised VEGFA protein levels after 24 hours of treatment (Figure 5a). PI3K levels had not been affected by lanthionine addition at both concentrations used, while a significant increase was observed in pAKT and pERK at 24 hours after 1 µM of lanthionine (Figure 5c). The levels of pERK appeared raised also at 48 hours of treatment with both concentrations used (Figure 5c). In HEK293 cells, lanthionine had no effect on VEGFA protein levels and on selected markers (Figure 5b, d).

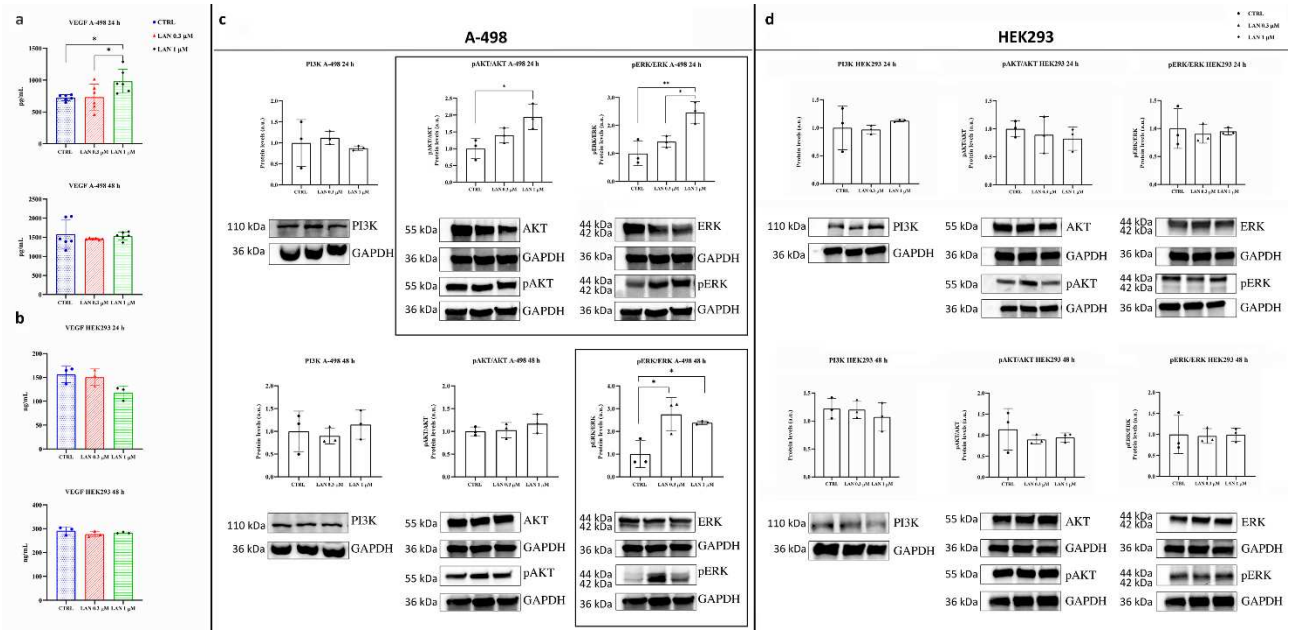


Figure 5. ELISA assay of VEGFA levels and western blot analysis of PI3K, pAKT/AKT and pERK/ERK.

(a) Analysis of VEGFA protein levels in A-498 cell culture medium after 24 and 48 hours of treatment with lanthionine at 0.3 µM and 1 µM. (b) Analysis of VEGFA protein levels in HEK293 cell culture medium after 24 and 48 hours of treatment with lanthionine at 0.3 µM and 1 µM. (c) Analysis on A-498 cells lysate after 24 and 48 hours of treatment with lanthionine at 0.3 µM and 1 µM. (d) Analysis on HEK293 cells lysate after 24 and 48 hours of treatment with lanthionine at 0.3 µM and 1 µM Histograms values are the mean ± standard deviation of three independent experiments: * $p \leq 0.05$, ** $p \leq 0.01$ and *** $p \leq 0.001$. CTRL: control; LAN 0.3 µM: lanthionine 0.3µM: LAN 1 µM: lanthionine 1 µM.

2.6 VEGF silencing influences cell migration and invasion in A-498 cells

The effect of lanthionine on cell migration was analyzed after VEGFA silencing only in A-498 cell line. After treating the cells with VEGF-siRNA for 24 hours, cell migration was evaluated after lanthionine treatment, from 0 to 24 hours, comparing the results obtained with respect to control. Considering the images in Fig. 6a and the analysis of the scratched area (%) in Fig. 6b, a significant reduction in the closure rate of the scratched area was detected. At 6 hours, the samples treated with VEGF-siRNA had a value of more than 60%, with a significant difference when comparing CTRL+VEGF-siRNA to the control or Scramble-siRNA, which had a value less than 50% (Figure 6a, b). This difference was also observed after 9 hours of treatment, where the scratch area of the control was reduced to about 30% (Figure 6a, b), while the samples treated with VEGF-siRNA had a value of about 50%. At 24 hours, the scratch area of samples treated with VEGF-siRNA was still evident, with a value of about 40%, with a significant difference with respect to control or scramble-siRNA samples, with a scratch area of about 20% (Figure 6a, b).

The analysis of VEGFA gene and protein levels was reported in Fig. 6c. As shown, VEGFA gene expression levels appeared reduced after transfection compared to control or scramble-siRNA. Considering protein levels, the transfection efficiency resulted in a clear reduction in VEGFA protein levels (Figure 6c).

Afterwards, the effect of lanthionine on cell invasion was analyzed following VEGFA silencing. Cells were transfected with VEGF-siRNA for 24 hours, and invasion was subsequently evaluated after 20 hours of lanthionine treatment.
Representative images (Figure 6d) and quantitative analysis of cell invasion (Figure 6e) revealed a significant reduction in cell invasion capacity upon VEGFA knockdown. Specifically, VEGF-siRNA-treated samples exhibited an approximately 50% decrease in cell invasion compared to the control (Figure 6e).

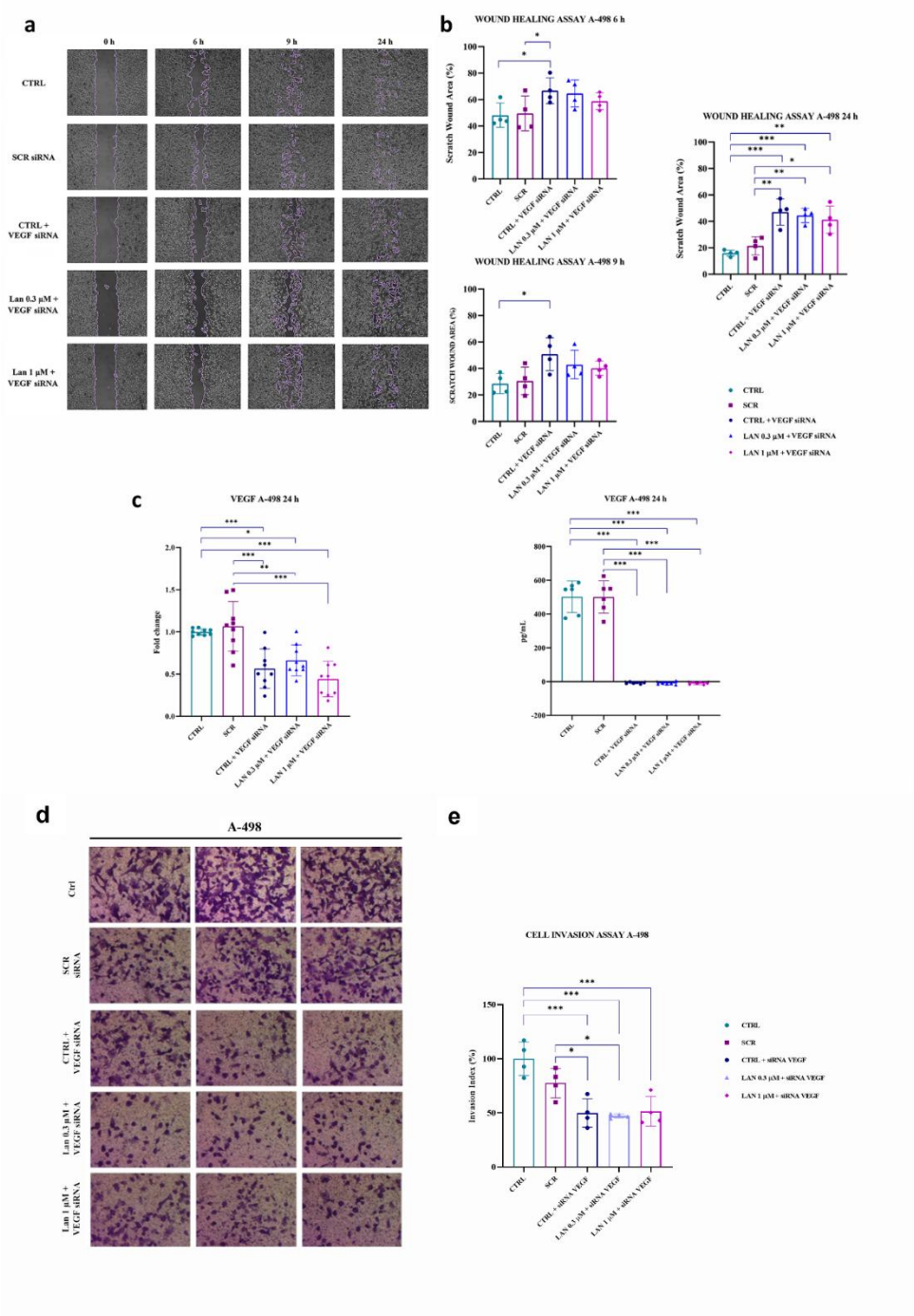


Figure 6. VEGF silencing influences cell migration and invasion in A-498 cells.
(a) Wound healing assay images acquired at 0, 6, 9 and 24 hours after treatment with 0.3 µM and 1 µM lanthionine in A-498 cells, post-VEGF-siRNA transfection. (b) Scratch wound area analysis, expressed as %, in A-498 cells at 6, 9 and 24 hours after treatment with 0.3 µM and 1 µM lanthionine in A-498 cells, post-VEGF-siRNA transfection. (c) VEGF gene and protein levels after 24 hours with

0.3 μM and 1 μM lanthionine in A-498 cells, post-VEGF-siRNA transfection. (d) Transwell invasion assay images acquired at 20 hours after treatment with 0.3 μM and 1 μM lanthionine in A-498 cells, post-VEGF-siRNA transfection. (e) Invasion index analysis, expressed as %, in A-498 cells at 20 hours after treatment with 0.3 μM and 1 μM lanthionine in A-498 cells, post-VEGF-siRNA transfection. Histograms values are the mean ± standard deviation of three independent experiments: * $p \leq 0.05$, ** $p \leq 0.01$ and *** $p \leq 0.001$. CTRL: control; SCR: scramble PCMT-siRNA; CTRL+VEGF-siRNA: control with VEGF-siRNA; LAN 0.3 μM + VEGF-siRNA: lanthionine 0.3μM with VEGF-siRNA; LAN 1 μM + VEGF-siRNA: lanthionine 1 μM + VEGF-siRNA.

2.7 VEGF silencing influences intracellular calcium levels and PI3K/AKT/mTOR signal pathway expression in A-498 cells

The effect of lanthionine on intracellular calcium levels and on PI3K/AKT/mTOR expression was analyzed after VEGFA silencing in A-498 cell line.

Intracellular calcium levels were reported in Fig. 7a. After VEGFA silencing, lanthionine did not increase the intracellular calcium levels, which instead appeared significantly reduced after 1, 3 and 6 hours of treatment.

PI3K/AKT/mTOR gene expression analysis were reported in Fig. 7b. Any significant increase of the genes selected were detected after VEGF-siRNA transfection, followed by lanthionine treatment, with a significant reduction mainly in mTOR gene expression levels.

However, HIF2A and HIF1B showed a significant increase. HIF2A appeared significantly higher than control considering both lanthionine concentrations utilized, while HIF1B only after adding 1 μM of lanthionine (Figure 7b).

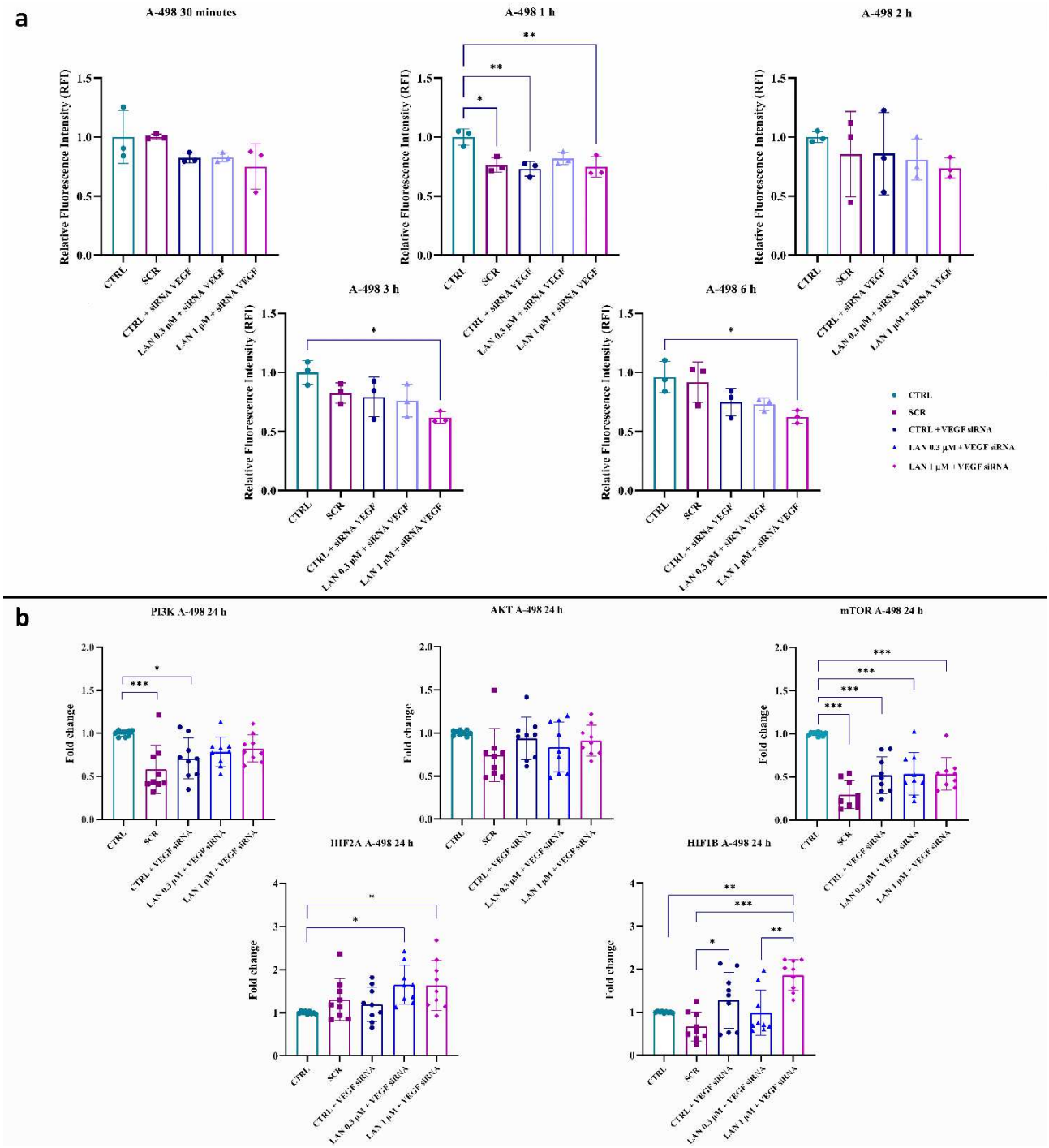


Figure 7. VEGF silencing influences intracellular calcium levels and PI3K/AKT/mTOR signaling pathway.

(a) Results obtained in A-498 cells after 30 minutes, 1, 2, 3 and 6 hours of treatments with 0.3 µM and 1 µM of lanthionine after VEGF-siRNA transfection. Results are expressed as relative fluorescence intensity (RFI). (b) PI3K/AKT/mTOR gene levels after 24 hours with 0.3 µM and 1 µM lanthionine in A-498 cells, post-VEGF-siRNA transfection. Histograms values are the mean ± standard deviation of three independent experiments: * $p \leq 0.05$, ** $p \leq 0.01$ and *** $p \leq 0.001$. CTRL: control; SCR: scramble PCMT -siRNA; CTRL+VEGF-siRNA: control with VEGF-siRNA; LAN 0.3 µM + VEGF-siRNA: lanthionine 0.3µM with VEGF-siRNA; LAN 1 µM + VEGF-siRNA: lanthionine 1 µM + VEGF-siRNA.

2.8 VEGF as a Specific Feature of Kidney Clear Cell Carcinoma (TCGA Data)

Considering the Cancer Genome Atlas (TGCA) database, VEGFA appears to be highly expressed especially in Kidney Renal clear cell carcinoma (KIRC), with respect to other cancer types (Figure 8 a), as well as respect to normal tissue (Figure 8 b, c).

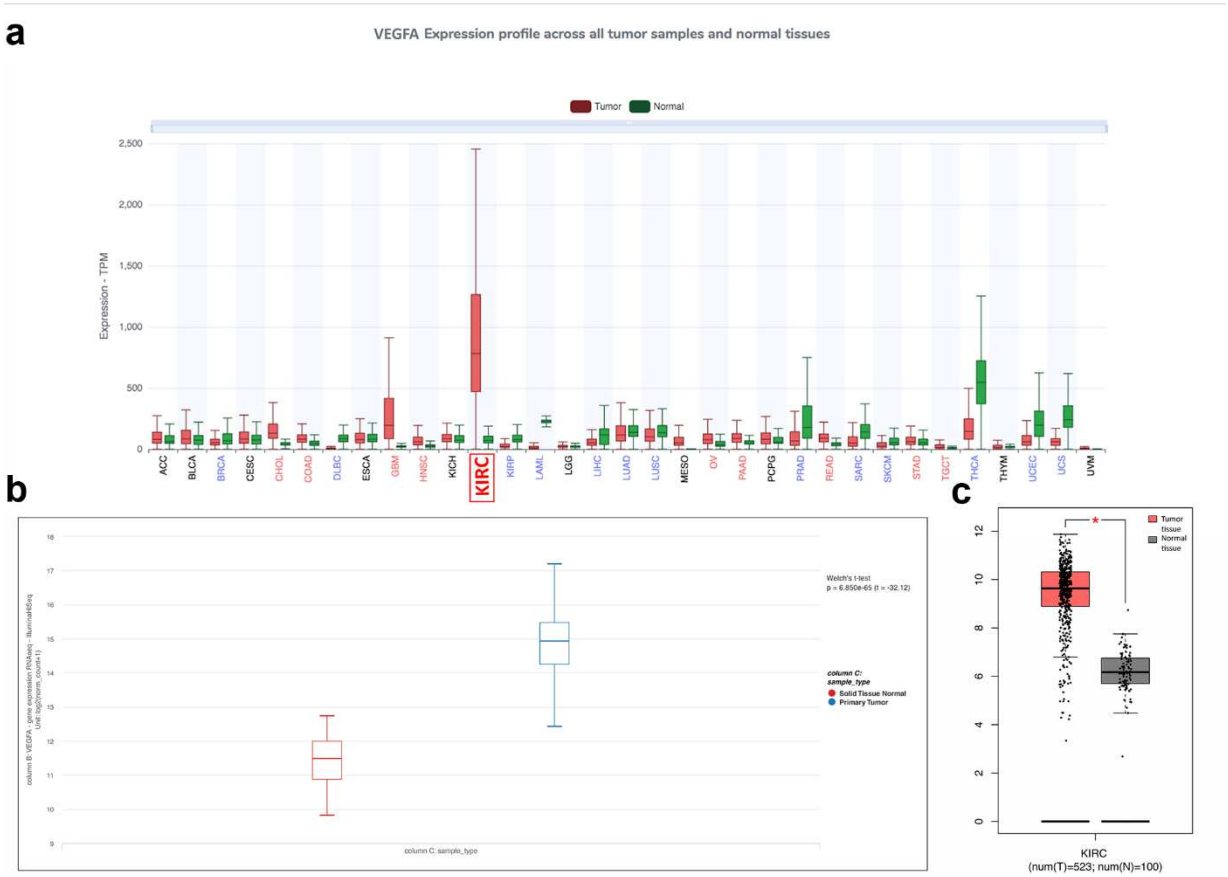


Figure 8. *VEGFA expression profile across all tumor samples and normal tissues.*
(a) VEGFA expression profile across tumor and normal tissue. KIRC: Kidney renal clear cell carcinoma, the other cancer acronyms are reported in supplementary table S1. (b) VEGFA gene expression profile in KIRC database analyzed by Xena browser (https://xenabrowser.net/). (c) VEGFA gene expression profile in KIRC database analyzed by GEPIA browser (http://gepia.cancer-pku.cn/).

3. Discussion

The present study provides preliminary evidence that lanthionine, at concentrations comparable to those detected in patients in CKD [25,29,30], exerts cell-specific effects on ccRCC cells.

Using A-498 ccRCC cell line and HEK293 cells as a comparative non-cancer model, our findings suggest that lanthionine enhances cell viability, migration, invasion, intracellular calcium signaling, and activation of the VEGF–PI3K/AKT/mTOR and HIFs axis, a pathway critically implicated in renal cancer progression. Importantly, VEGFA silencing attenuated lanthionine-induced migration and invasion and abolished the associated increase in intracellular Ca^{2+}, supporting a functional role for VEGFA in the cellular response to lanthionine.

Wound healing and invasion assay showed that lanthionine promotes A-498 cell migration and invasive capacity in a dose- and time- dependent manner. This effect was prominently observed in cancer cells, where most of the scratches were closed within 9 hours of treatment. However, lanthionine exerted only a mild effect on HEK293 cells, with a complete scratch closure after 24 hours (Figure 1a-d). Similar results were obtained evaluating cell invasive capacity; lanthionine treatment selectively induces a significant, dose-dependent increase in cancer cell invasion, whereas non-tumor cells maintained their baseline behavior (Figure 2a-d).

Cell migration and invasion are critical processes driven by complex intracellular signaling cascades and microenvironmental factors such as chemokine, cell adhesion molecules and cytokines [32–34]. Our results indicate that lanthionine acts as a selective driver of cancer cell aggressiveness. The rapid onset of cell motility observed in the wound healing assay- which began as early as 9 hours and culminated in complete closure at 24 hours-suggests that lanthionine may trigger an immediate signaling cascade that drives the migration mechanism. This enhanced motility was complemented by a significant increase in cell invasive capacity at 20 hours. The markedly weaker response observed in HEK293 cells suggests that the effects of lanthionine may depend on the cellular context and the molecular features of ccRCC cells. Similar pro-migratory and -invasive effects have been described for other UTs, including *p*-cresyl sulfate and indoxyl sulfate [21–23,35]. Our data extends this concept by identifying lanthionine as an additional uremic metabolite capable of enhancing cancer cell migration and invasion.

Previous results showed that lanthionine increased intracellular calcium levels in endothelial cells [27,30], so the levels of this second messenger were analyzed also in these cell models. We found a dose-dependent increase in the intracellular calcium levels induced by lanthionine, exclusively in A-498 cells (Figure 3a, b). The regulation of intracellular calcium levels is crucial to several cellular processes, including proliferations, migration and gene transcription. In cancer cells, aberrant calcium signaling supports enhanced survival, invasion and metastasis, contributing to rewiring of intracellular signaling networks to regulate cell migration modules [36].

As previously mentioned, A-498 cells presented a highly vascular phenotype, associated with an elevated expression of VEGFA, also known as vascular endothelial growth factor A [37].

VEGFA exhibits its effect through the interaction with transmembrane tyrosine-kinase receptors (VEGFRs), expressed by endothelial cells to promote angiogenesis and migratory mechanisms [37,38]. In addition to its established role in angiogenesis, VEGFA can participate in autocrine and paracrine signaling within the tumor microenvironment and has been linked to intracellular Ca^{2+} mobilization and pathways regulating tumor cell migration and invasion [39–42].

Given the central role of VEGFA in ccRCC and the established interaction between VEGFA signaling and intracellular Ca^{2+} dynamics, we next examined whether lanthionine could modulate this pathway. Our results show that in A-498 cells, lanthionine increased VEGFA at both transcriptional (Figure 4a, b) and protein levels (Figure 5a), particularly at 1 μM, whereas no comparable increase was observed in HEK293 cells. Interestingly, beyond its involvement in promoting cancer, elevated

circulating VEGFA levels have also been associated with inflammatory state and mortality in CKD patients [29,43–45]. In addition, VEGFA itself may act as a proinflammatory cytokine, increasing endothelial cell permeability with an altered expression of endothelial cell adhesion molecules and chemokines [46,47]. This could represent a further link between CKD and kidney cancer.

In our experimental set, lanthionine also promotes the VEGF downstream PI3K/AKT/mTOR signaling pathway in A-498 cells, after 48 hours, with increased expression of PI3K, AKT, mTOR-related genes (Figure 4a, b) and increased pAKT protein levels under specific experimental conditions (Figure 5c).

A significant crosstalk exists between VHL-HIF-VEGF, intracellular calcium and PI3K/AKT/mTOR pathways, which synergistically promote renal cancer cell progression [35,48–50]. In addition, it should be noted that genetic alterations in signaling are highly significant in ccRCC, the abnormal activation of PI3K/AKT/mTOR correlates with aggressive development invasion and metastasis in ccRCC [49–51]. About the results obtained in HEK293 cells, we have found an increase only in mTOR after 1 μM of lanthionine at 48 hours of treatment (Figure 4c, d).

Due to VHL inactivation, ccRCC is characterized by a HIF-α stabilization even in a normoxic condition, resulting in the activation of HIF target genes, as well as VEGF overexpression, that influence and modify several cellular processes such as angiogenesis, proliferation and cell metabolism [52,53]. Our results demonstrated that 1 μM lanthionine induced a significant increase in HIF2A and HIF1B expression in A-498 cells up to 48 hours (Figure 4a, b). In HEK293, 1 μM of lanthionine increased HIF2A expression at 48 hours, while both concentrations promoted HIF1B at the same time of treatment (Figure 4c, d).

HIF2A is strictly involved in oxidative stress, and vascular remodeling [54]. Importantly, HIF-2α selectively drives VEGFA transcription, lipid metabolism, and cell cycle progression in ccRCC, distinguishing it from the more glycolysis-oriented HIF-1α [55]; additionally, it is involved in ccRCC progression and metastasis [56]. One possible explanation is that lanthionine, as UT, may perturb cellular redox or metabolic homeostasis, thereby influencing hypoxia-related signaling [57,58].

Indeed, alterations in HIFs caused by UTs were already observed evaluating the effect of pCS on ccRCC cells [24], supporting the idea that uremic toxicity can exacerbate hypoxia-driven tumor signaling.

Regarding the results obtained by the ELISA and western blotting analysis, we found significant changes in the protein levels of VEGFA after 24 hours of treatment with 1 μM of lanthionine in A-498 cells compared to HEK293 (Figure 5a, b). Differences were also observed in pAKT and pERK levels under the same conditions (Figure 5c), while no differences were found in HEK293 cells (Figure 5d). These data are fully consistent with molecular data, both for the cell-specificity effect of lanthionine and for the modulated pathway. Indeed, activated pERK is also a downstream effector of VEGFA signaling, involved in tumor invasiveness, growth and angiogenesis. Studies demonstrated that analyzing pERK activity in RCC biopsy could become useful for creating targeted and personalized therapy [59].

Afterwards, to confirm the observed cell-specific activity of lanthionine on VEGF-PI3K/AKT/mTOR pathway, we performed a VEGFA knockdown, by transfecting A-498 cells with siRNA against human VEGFA. The success of the transfection was verified by evaluating both VEGFA gene expression and protein levels, which appeared visibly reduced (Figure 6c).

VEGFA silencing substantially attenuated the effects of lanthionine on A-498 cells, reducing migration (Figure 6a, b), invasion (Figure 6d, e), and abolishing the lanthionine-induced increase in intracellular Ca^{2+} (Figure 7a). VEGFA knockdown was also associated with reduced expression of components of the PI3K/AKT/mTOR pathway, particularly mTOR (Figure 7b). Together, these findings support a functional role for VEGFA in mediating the cellular response to lanthionine.

Notably, HIFs expression remained elevated after VEGFA silencing, suggesting that lanthionine may act upstream of VEGFA, possibly by inducing hypoxia-like stress or metabolic imbalance, which in turn, activates HIFs transcription independently of VEGFA feedback [60].
The relevance of VEGFA to ccRCC was further supported by our analysis of publicly available TCGA/KIRC datasets, in which VEGFA expression was markedly elevated in KIRC compared with normal renal tissue and was prominent relative to several other tumor types (Figure 8a-c). These data provide an independent clinical-genomic context for our *in vitro* observation that lanthionine increases VEGFA expression in A-498 cells.
Overall, our findings identify lanthionine as a previously unexplored uremic metabolite capable of modulating numerous key genes involved in ccRCC progression, in a cell-specific manner, through VEGF-dependent signaling. This observation underscores the translational relevance of these findings. Indeed, lanthionine may represent one of the molecular links between renal dysfunction and kidney cancer progression, but also a putative biomarker. Whether circulating or urinary lanthionine levels are associated with ccRCC incidence, progression, or severity in patients with CKD remains unknown and warrants dedicated clinical investigation.

4. Conclusion

This study provides the first experimental evidence that lanthionine, at CKD-relevant concentrations, exerts a pro-tumorigenic and cell-specific effect in A-498 ccRCC. Our findings show that lanthionine is involved in the promotion of ccRCC migration and invasion, through calcium/VEGF-dependent signaling, representing a putative mechanistic link between CKD and kidney cancer. Indeed, VEGF silencing abolished lanthionine-induced calcium signaling and migratory responses, identifying VEGF as a central mediator connecting lanthionine exposure with Ca^{2+} signaling and downstream pathways associated with ccRCC promotion.
Although limited to an *in vitro* model, this work throws the foundation for future studies, aimed at defining the role of lanthionine, as well as other UTs, in cancer biology, and evaluating lanthionine as a potential biomarker in CKD-associated malignancies.

5. Methods

5.1 Cell Culture

A-498 and HEK293 cells (ATCC) were cultured in DMEM media, supplemented with 10% FBS Fetal Bovine Serum (S1810-500, Microtech, Pozzuoli, NA, Italy), 2 mM L-glutamine (X0550-100, Microtech, Pozzuoli, NA, Italy) and 0.1% penicillin–streptomycin (L0022-100, Microtech, Pozzuoli, NA, Italy), maintained in a humidified atmosphere containing 5% CO_2 at 37 °C.

5.2 Experimental Design

Cells were treated one day after seeding with 0.3 or 1 μM DL-lanthionine (Lan, L8543, Sigma Aldrich, Merck KGaA, Darmstadt, Germany) for 24 and 48 hours. DL -lanthionine was dissolved in 1M HCl in water at a stock concentration of 50 mg/mL (240 mM). The vehicle effect, corresponding to HCl addition to DMEM, was considered negligible, as no detectable changes in pH or cell vitality could be detected. Control cultures were maintained in standard lanthionine-free medium.

5.3 MTT assay

Cell viability were measured using MTT assay, according to the manufacturer's instruction. This assay was based on the ability of living cells to reduce MTT in blue- violet formazan crystals. Briefly, cells were seeded in 96-well plates at the proper density and allowed to adhere for 24 hours. Subsequently, they were incubated in medium containing 1% FBS, with lanthionine added in

triplicate, at concentrations of 0.3 and 1 μM for 24 and 48 hours. Thereafter, the medium was removed, and the cultures were treated with MTT (M2128 Sigma Aldrich, Merck KGaA, Darmstadt, Germany) dissolved in PBS (ML116 HIMEDIA Laboratory GMmbH, Modautal, Germany) at a final concentration of 0.5 mg/mL for 4 hours at 37 °C. Following incubation, the medium containing the MTT solution was aspirated from the wells, and the remaining formazan crystals were solubilized in 1N isopropanol/hydrochloric acid (10%) solution, using a shaker for 20 min.
Absorbance was then measured at 570 nm using a 96 well microplate reader (Bio-Rad Laboratories, Milan, Italy). The cytotoxicity index was determined using the untreated cells as the negative control. Data are presented as mean ± standard deviation from three different experiments, performed in triplicate.

5.4 Wound healing assay

Cells from each line were seeded in 6-well culture plates using Ibidi Culture-Insert 2 Well, according to the manufacturer's protocol (Ibidi GmbH, Gräfelfing, Germany).
After 24 hours, an optically confluent cell monolayer was established. The inserts were then removed, and the corresponding treatments were applied in medium supplemented with 1% FBS. The substrates containing confluent cell layers were imaged starting at 0 hours (treatment initiation) and monitored for up to 24 hours, until closure of the scratch area. Images were acquired every 6 hours using Optika camera software and observed by a LEICA DM-IRB photomicroscope at 1×/5× magnification. Image analysis was performed using ImageJ to quantify the gap closure by measuring the scratch area over time. Data are presented as scratch wound area (%) relative to the control ± standard deviation (SD), based on three different experiments.

5.5 Cell invasion assay

Cell invasion capacity was analyzed using 12-well Nunc™ Cell Culture Inserts in Carrier Plate Systems with 8 μm pore size (Thermo Fisher Scientific, Waltham, Massachusetts, USA), according to the manufacturer's protocol.
The inserts were coated with Geltrex LDEV-Free Reduced Growth Factor Basement Membrane Matrix. Following a 24-hours starvation period in serum-free DMEM, cells were seeded into the upper chambers. DMEM supplemented with 10% FBS, either with or without lanthionine, was added to the bottom well as chemoattractant medium, for 20 hours at 37 °C with 5% CO_2.
Following the incubation, non-invaded cells on the upper surface of the membrane were removed and invaded cells on the lower surface were then fixed, stained with crystal violet solution and visualized by a LEICA DM-IRB photomicroscope at 1×/10× magnification. Image analysis was performed using ImageJ to quantify the number of invasive cells. Data are presented as invasion index (%) relative to the control ± standard deviation (SD), based on three different experiments.

5.6 Intracellular calcium analysis

Intracellular calcium analysis was performed using a fluorescent Fura 2-AM probe (F1201, ThermoFisher Scientific, Waltham, Massachusetts, USA), following the supplier's protocol. Cells from each line were seeded in 12-well culture plates. After 24 hours, culture medium was removed, and incubated with lanthionine added in triplicate, at concentrations of 0.3 and 1 μM for 30 minutes, 1, 2, 3 and 6 hours, respectively. After each time point, 3 μM of the probe dissolved in PBS was added for 50 minutes at 37 °C in a humidified atmosphere enriched with 5% CO_2.
Fluorescence intensity was quantified at λE_x340 nm and λE_m510 nm by a fluorescence multi-reader (Infinite 200, Tecan Trading AG, Männedorf, Switzerland). Intracellular calcium concentration was expressed as relative fluorescence intensity (RFI), considering the untreated cells as negative control.

5.7 RNA Extraction, Reverse Transcription and qPCR

Total mRNA was extracted from cells using TRI reagent (Sigma Aldrich, Merck KGaA, Darmstadt, Germany) according to the manufacturer 's instructions. RNA concentration was determined with NanoDrop UV/Vis micro-spectrophotometer (Life Real, Zhejiang, China). Samples were stored at −80 °C until further use. A total of 2 µg of total RNA was reverse transcribed using the QuantiTect Reverse Transcription® kit 5× All-in-One RT Mastermix (G486, ABM, Richmond, BC, Canada), following the manufacturer's instructions. Reactions were carried out in a Veriti® 96-Well Thermal Cycler (Applied Biosystems, Foster City, CA, USA). The resulting cDNA concentration was measured by means of NanoDrop UV/Vis micro-spectrophotometer and samples were stored at −20 °C until useQuantitative PCR (qPCR) was performed with 200 ng of cDNA using Luna universal qPCR Master Mix (M3003X, New England Biolabs, Ipswich, Massachusetts, USA) on a CFX96 Touch Real-Time PCR Detection System (BioRad, CA, USA). Target-specific primers for PI3K, AKT, mTOR, VEGFA, HIF2A, HIF1B and GAPDH were designed with Primer-BLAST software (https://www.ncbi.nlm.nih.gov/tools/primer-blast/) and synthesized by Life Technologies (Thermofisher Scientific, Waltham, Massachusetts, USA). All reactions were performed in triplicate under amplification conditions specified by the manufacturer. Relative gene expression was calculated using the $2^{-\Delta\Delta Ct}$ method, with GAPDH as housekeeping gene. Primer sequences are listed in Table 1.

Gene	Primer reverse	Primer forward
PIK3CA (PI3K)	GAAGCACCTGAATAGGCAAGTCG	GAGCATCCATGAAATCTGGTCGC
AKT1 (AKT)	GAGCATCCATGAAATCTGGTCGC	ATGGCGCTGAGATTGTG
mTOR	CGGGCACTCTGCTCTTT	GGCCGACTCAGTAGCAT
VEGFA	TGCATTCACATTTGTTGTGCTGTAG	TGCAGATTATGCGGATCAAACC
EPAS1 (HIF2A)	TTGTCACACCTATGGCATATCACA	GTGCTCCCACGGCCTGTA
ARNT (HIF1B)	GAGGGGCTAGGCCACTATTC	CAAGCCCCTTGAGAAGTCAG

Table. 1. Primer sequences used in qPCR analysis. PI3K: phosphatidylinositol-4,5-bisphosphate 3-kinase, catalytic subunit alpha; AKT: AKT serine/threonine kinase 1; mTOR: mechanistic target of rapamycin; VEGF: vascular endothelial growth factor A; EPAS1(HIF2A): Endothelial PAS domain-containing protein 1; ARNT (HIF1B): Aryl Hydrocarbon Receptor Nuclear Translocator.

5.8 Elisa assay

ELISA kits for human VEGF (DVE00) were obtained from R&D Systems (Minneapolis, USA) and used according to manufacturer 's instructions. Absorbance was measured with a multi-reader (Infinite 200, Tecan Trading AG, Männedorf, Switzerland). All the experiments were performed in triplicate.

5.9 Protein Extraction and Western Blotting analysis

Cells were collected and lysed in RIPA buffer (TCL131, HIMEDIA Laboratory GMmbH, Modautal, Germany) supplemented with a cocktail of protease inhibitors (cat. n°11836153001, Roche, Milan, Italy) and phosphatase inhibitors (4906845001, Sigma Aldrich, Merck KGaA, Darmstadt, Germany).

Protein concentrations were determined using the Bradford Protein Assay Kit (5000001, BioRad, Hercules, CA, USA). Proteins were separated by electrophoresis on 8–16% precast gels (456-1104, mini-PROTEANS® TGX™ Gels, Bio-Rad, Hercules, CA, USA) and transferred onto 0.2 μm nitrocellulose membranes (1704158, Trans-Blot® Turbo™, Bio-Rad, Hercules, CA, USA).
Proteins immunodetection was performed using the following primary antibodies: anti-PI3K (4249, Cell Signaling Technology, Danvers, MA, USA), anti-AKT (4691, Cell Signaling Technology, Danvers, MA, USA), anti-pAKT (4060, Cell Signaling Technology, Danvers, MA, USA), anti-ERK (9102, Cell Signaling Technology, Danvers, MA, USA), anti-pERK (4370, Cell Signaling Technology, Danvers, MA, USA) and anti-GAPDH (GTX100118-S, Genetex, CA, USA), as loading controls. Secondary antibodies included horseradish peroxidase (HRP)- conjugated anti-rabbit (NC27606, Immunoreagents Inc., Raleigh, NC, USA) and anti-mouse (Immunoreagents Inc., Raleigh, NC, USA).
Immune complexes were detected by chemiluminescence utilizing Immobilon Western Chemiluminescent HRP Substrate (WBKLS0500, Millipore Corporation, Billerica, MA, USA) and visualized with a transilluminator (ChemiDoc™, Bio-Rad, CA, USA). Signal intensities were quantified with Image Lab software. All the experiments were performed in triplicate.

5.10 siRNA transfection of A-498 cell line

To inhibit VEGFA protein expression, siRNA transfection was performed in the A-498 cell line using lipofectamine RNAiMAX. Transfection Reagent (Thermo Fisher Scientific Inc. cat n° 13778075, Waltham, Massachusetts, USA) was used following manufacturer's instructions.

Five different conditions were established:

1. CTRL: cells without siRNA transfection;
2. Scramble: cells transfected with a non-targeting control siRNA (i.e. Flexi tube siRNA against human PCMT, Qiagen, cat n° 1027416, Hilden, Germany);
3. VEGF siRNA cells transfected with siRNA targeting human VEGF (Qiagen, cat n° 1027416, Hilden, Germany);
4. Lan 0.3 μM + VEGF siRNA: same as VEGF siRNA condition, with 0.3 μM lanthionine added 24 hours post-transfection;
5. Lan 1 μM + siRNA VEGF: same as VEGF siRNA condition, with 1 μM lanthionine added 24 hours post-transfection.

Data are presented as mean ± SD from three independent experiments, each performed in triplicate.

5.11 Statistical Analysis

Data are expressed as the means ± SD, except where otherwise specified. The results were analyzed using the statistics software GraphPad Prism Version 5.0 (GraphPad Software, San Diego, CA, USA). Statistical significance was determined as * $p \leq 0.05$, ** $p \leq 0.01$ and *** $p \leq 0.001$ using one-way ANOVA test.

References

1. Jager, K. J. *et al.* A single number for advocacy and communication—worldwide more than 850 million individuals have kidney diseases. *Nephrology Dialysis Transplantation* **34**, 1803–1805 (2019).
2. Lo, R., Narasaki, Y., Lei, S. & Rhee, C. M. Management of traditional risk factors for the development and progression of chronic kidney disease. *Clinical Kidney Journal* **16**, 1737–1750 (2023).
3. Mark, P. B. *et al.* Global, regional, and national burden of chronic kidney disease in adults, 1990–2023, and its attributable risk factors: a systematic analysis for the Global Burden of Disease Study 2023. *The Lancet* **406**, 2461–2482 (2025).
4. Falconi, C. A. *et al.* Uremic Toxins: An Alarming Danger Concerning the Cardiovascular System. *Front. Physiol.* **12**, 686249 (2021).
5. Major, R. W. *et al.* Cardiovascular disease risk factors in chronic kidney disease: A systematic review and meta-analysis. *PLoS One* **13**, e0192895 (2018).
6. Vanholder, R. *et al.* Review on uremic toxins: Classification, concentration, and interindividual variability. *Kidney International* **63**, 1934–1943 (2003).
7. Lisowska-Myjak, B. Uremic Toxins and Their Effects on Multiple Organ Systems. *Nephron Clin Pract* **128**, 303–311 (2014).
8. Coppola, A. *et al.* Zebrafish as a Model of Cardiac Pathology and Toxicity: Spotlight on Uremic Toxins. *IJMS* **24**, 5656 (2023).
9. El Chamieh, C., Liabeuf, S. & Massy, Z. Uremic Toxins and Cardiovascular Risk in Chronic Kidney Disease: What Have We Learned Recently beyond the Past Findings? *Toxins (Basel)* **14**, 280 (2022).
10. Lekawanvijit, S. Cardiotoxicity of Uremic Toxins: A Driver of Cardiorenal Syndrome. *Toxins (Basel)* **10**, 352 (2018).
11. Perna, A. *et al.* Zebrafish, a Novel Model System to Study Uremic Toxins: The Case for the Sulfur Amino Acid Lanthionine. *IJMS* **19**, 1323 (2018).
12. Cooper, B. A. *et al.* A Randomized, Controlled Trial of Early versus Late Initiation of Dialysis. *N Engl J Med* **363**, 609–619 (2010).
13. Dogan, E. *et al.* Incidence of renal insufficiency in cancer patients. *Adv Therapy* **22**, 357–362 (2005).

14. Larcher, A. *et al.* Epidemiology of Renal Cancer: Incidence, Mortality, Survival, Genetic Predisposition, and Risk Factors. *European Urology* **88**, 341–358 (2025).
15. Bukavina, L. *et al.* Epidemiology of Renal Cell Carcinoma: 2022 Update. *European Urology* **82**, 529–542 (2022).
16. Perazella, M. A., Dreicer, R. & Rosner, M. H. Renal cell carcinoma for the nephrologist. *Kidney International* **94**, 471–483 (2018).
17. Jonasch, E., Gao, J. & Rathmell, W. K. Renal cell carcinoma. *BMJ* **349**, g4797–g4797 (2014).
18. Saly, D. L., Eswarappa, M. S., Street, S. E. & Deshpande, P. Renal Cell Cancer and Chronic Kidney Disease. *Advances in Chronic Kidney Disease* **28**, 460-468.e1 (2021).
19. Clark, P. E. The role of VHL in clear-cell renal cell carcinoma and its relation to targeted therapy. *Kidney International* **76**, 939–945 (2009).
20. Di Paola, R. *et al.* Possible Effects of Uremic Toxins p-Cresol, Indoxyl Sulfate, p-Cresyl Sulfate on the Development and Progression of Colon Cancer in Patients with Chronic Renal Failure. *Genes* **14**, 1257 (2023).
21. Chen, X. *et al.* Effects of p-cresol, a uremic toxin, on cancer cells. *Transl Cancer Res* **12**, 367–374 (2023).
22. Ichisaka, Y., Yano, S., Nishimura, K., Niwa, T. & Shimizu, H. Indoxyl sulfate contributes to colorectal cancer cell proliferation and increased EGFR expression by activating AhR and Akt. *Biomed. Res.* **45**, 57–66 (2024).
23. Saito, S., Koya, Y., Kajiyama, H., Yamashita, M. & Nawa, A. Indoxyl Sulfate Promotes Metastatic Characteristics of Ovarian Cancer Cells via Aryl Hydrocarbon Receptor–Mediated Downregulation of the Mas Receptor. *Laboratory Investigation* **103**, 100025 (2023).
24. Tanimoto, K. Mechanism of regulation of the hypoxia-inducible factor-1alpha by the von Hippel-Lindau tumor suppressor protein. *The EMBO Journal* **19**, 4298–4309 (2000).
25. Perna, A. F. *et al.* Divergent behavior of hydrogen sulfide pools and of the sulfur metabolite lanthionine, a novel uremic toxin, in dialysis patients. *Biochimie* **126**, 97–107 (2016).
26. Perna, A. F., Zacchia, M., Trepiccione, F. & Ingrosso, D. The Sulfur Metabolite Lanthionine: Evidence for a Role as a Novel Uremic Toxin. *Toxins (Basel)* **9**, 26 (2017).

27. Vigorito, C. *et al.* Uremic Toxin Lanthionine Interferes with the Transsulfuration Pathway, Angiogenetic Signaling and Increases Intracellular Calcium. *IJMS* **20**, 2269 (2019).
28. Perna, A. F. *et al.* Lanthionine and Other Relevant Sulfur Amino Acid Metabolites: Detection of Prospective Uremic Toxins in Serum by Multiple Reaction Monitoring Tandem Mass Spectrometry. *Methods Mol Biol* **2007**, 9–17 (2019).
29. Perna, A. F. *et al.* Lanthionine, a Novel Uremic Toxin, in the Vascular Calcification of Chronic Kidney Disease: The Role of Proinflammatory Cytokines. *IJMS* **22**, 6875 (2021).
30. Coppola, A. *et al.* Uremic Toxin Lanthionine Induces Endothelial Cell Mineralization In Vitro. *Biomedicines* **10**, 444 (2022).
31. Hellmich, M. R. *et al.* Efficacy of Novel Aminooxyacetic Acid Prodrugs in Colon Cancer Models: Towards Clinical Translation of the Cystathionine β-Synthase Inhibition Concept. *Biomolecules* **11**, 1073 (2021).
32. Friedl, P. & Alexander, S. Cancer Invasion and the Microenvironment: Plasticity and Reciprocity. *Cell* **147**, 992–1009 (2011).
33. Janiszewska, M., Primi, M. C. & Izard, T. Cell adhesion in cancer: Beyond the migration of single cells. *Journal of Biological Chemistry* **295**, 2495–2505 (2020).
34. Novikov, N. M., Zolotaryova, S. Y., Gautreau, A. M. & Denisov, E. V. Mutational drivers of cancer cell migration and invasion. *Br J Cancer* **124**, 102–114 (2021).
35. Hsu, Y.-H., Huang, H.-P. & Chang, H.-R. The uremic toxin p-cresol promotes the invasion and migration on carcinoma cells via Ras and mTOR signaling. *Toxicology in Vitro* **58**, 126–131 (2019).
36. Tsai, F.-C., Kuo, G.-H., Chang, S.-W. & Tsai, P.-J. Ca^{2+} Signaling in Cytoskeletal Reorganization, Cell Migration, and Cancer Metastasis. *BioMed Research International* **2015**, 1–13 (2015).
37. Pal, K. *et al.* Synchronous inhibition of mTOR and VEGF/NRP1 axis impedes tumor growth and metastasis in renal cancer. *npj Precis. Onc.* **3**, 31 (2019).
38. Li, H. & Huang, X. Advances in the molecular signaling mechanisms of VEGF/VEGFR2 in fundus neovascularization disease (Review). *Exp Ther Med* **30**, 1–13 (2025).
39. Hamerlik, P. *et al.* Autocrine VEGF–VEGFR2–Neuropilin-1 signaling promotes glioma stem-like cell viability and tumor growth. *Journal of Experimental Medicine* **209**, 507–520 (2012).

40. Lichtenberger, B. M. *et al.* Autocrine VEGF Signaling Synergizes with EGFR in Tumor Cells to Promote Epithelial Cancer Development. *Cell* **140**, 268–279 (2010).
41. Wu, P.-H. *et al.* The relationship of indoxyl sulfate and p-cresyl sulfate with target cardiovascular proteins in hemodialysis patients. *Sci Rep* **11**, 3786 (2021).
42. Goel, H. L. & Mercurio, A. M. VEGF targets the tumour cell. *Nat Rev Cancer* **13**, 871–882 (2013).
43. Boursiquot, B. C., Zabor, E. C., Glezerman, I. G. & Jaimes, E. A. Hypertension and VEGF (Vascular Endothelial Growth Factor) Receptor Tyrosine Kinase Inhibition: Effects on Renal Function. *Hypertension* **70**, 552–558 (2017).
44. Mazidi, M. *et al.* VEGF, the underlying factor for metabolic syndrome; fact or fiction? *Diabetes & Metabolic Syndrome: Clinical Research & Reviews* **11**, S61–S64 (2017).
45. Catar, R. *et al.* Expanded Hemodialysis Therapy Ameliorates Uremia-Induced Systemic Microinflammation and Endothelial Dysfunction by Modulating VEGF, TNF-α and AP-1 Signaling. *Front. Immunol.* **12**, 774052 (2021).
46. Patel, S. A. *et al.* Molecular Mechanisms and Future Implications of VEGF/VEGFR in Cancer Therapy. *Clinical Cancer Research* **29**, 30–39 (2023).
47. Reinders, M. E. J. *et al.* Proinflammatory functions of vascular endothelial growth factor in alloimmunity. *J. Clin. Invest.* **112**, 1655–1665 (2003).
48. Gargalionis, A. N. *et al.* Polycystin-1 induces activation of the PI3K/AKT/mTOR pathway and promotes angiogenesis in renal cell carcinoma. *Cancer Letters* **489**, 135–143 (2020).
49. Jiang, A. *et al.* Renal cancer: signaling pathways and advances in targeted therapies. *MedComm* **5**, e676 (2024).
50. Guo, Y. *et al.* ERK/MAPK signalling pathway and tumorigenesis (Review). *Exp Ther Med* https://doi.org/10.3892/etm.2020.8454 (2020) doi:10.3892/etm.2020.8454.
51. Twardowski, P. W., Mack, P. C. & Lara, P. N. Papillary Renal Cell Carcinoma: Current Progress and Future Directions. *Clinical Genitourinary Cancer* **12**, 74–79 (2014).
52. Maxwell, P. H. *et al.* Hypoxia-inducible factor-1 modulates gene expression in solid tumors and influences both angiogenesis and tumor growth. *Proc. Natl. Acad. Sci. U.S.A.* **94**, 8104–8109 (1997).

53. Strikic, A. *et al.* Differential expression of HIF1A and its downstream target VEGFA in the main subtypes of renal cell carcinoma and their impact on patient survival. *Front. Oncol.* **13**, 1287239 (2023).

54. Schödel, J. *et al.* High-resolution genome-wide mapping of HIF-binding sites by ChIP-seq. *Blood* **117**, e207–e217 (2011).

55. Samanta, D. & Semenza, G. L. Metabolic adaptation of cancer and immune cells mediated by hypoxia-inducible factors. *Biochimica et Biophysica Acta (BBA) - Reviews on Cancer* **1870**, 15–22 (2018).

56. Choi, W. S. W., Boland, J. & Lin, J. Hypoxia-Inducible Factor-2α as a Novel Target in Renal Cell Carcinoma. *J Kidney Cancer VHL* **8**, 1–7 (2021).

57. Chiang, C.-K., Tanaka, T. & Nangaku, M. Dysregulated Oxygen Metabolism of the Kidney by Uremic Toxins: Review. *Journal of Renal Nutrition* **22**, 77–80 (2012).

58. Hamza, E., Metzinger, L. & Metzinger-Le Meuth, V. Uremic Toxins Affect Erythropoiesis during the Course of Chronic Kidney Disease: A Review. *Cells* **9**, 2039 (2020).

59. Hoerner, C. R. *et al.* Multiregion Quantification of Extracellular Signal-regulated Kinase Activity in Renal Cell Carcinoma. *European Urology Oncology* **3**, 360–364 (2020).

60. Kamura, T. *et al.* Activation of HIF1α ubiquitination by a reconstituted von Hippel-Lindau (VHL) tumor suppressor complex. *Proc. Natl. Acad. Sci. U.S.A.* **97**, 10430–10435 (2000).

Funding

This research was funded by EUTox, the European Uremic Toxins work group.

Author information and Affiliations

Department of Precision Medicine, University of Campania Luigi Vanvitelli, Naples, Italy
Annapaola Coppola, Patrizia Lombari, Christian Di Maro, Antonio D'Andrea, Diego Ingrosso

Department of Experimental Medicine, University of Campania, Luigi Vanvitelli, Naples, Italy
Diana Ingrosso

Department of Translational Medical Science, University of Campania Luigi Vanvitelli, Naples, Italy
Giovanna Capolongo, Mariadelina Simeoni, Alessandra F. Perna

Department of Psychology and Health Science, Pegaso University, Naples, Italy
Margherita Borriello

Contributions

A C: conceptualization, data curation, formal analysis, investigation, methodology, visualization, writing – original draft, writing – review and editing. **P. L.** conceptualization, data curation, formal analysis, investigation, methodology, visualization, writing – original draft, writing – review and editing. **C.D.M.**: data curation, formal analysis, methodology, original draft, writing. **A. D.**: methodology, original draft, writing. **G. C.**: funding acquisition, review and editing. **M. S.**: visualization, writing – review and editing. **A. F. P**: conceptualization, visualization, supervision, writing – original draft, writing – review and editing. **D. I.**: conceptualization, visualization, supervision, writing – original draft, writing – review and editing. **M. B.**: conceptualization, investigation, visualization, supervision, writing – original draft, writing – review and editing.

Corresponding author

Correspondence to margherita.borriello@unicampania.it

Competing interests

The authors declare no competing interests.

Data availability

The datasets generated during and/or analysed during the current study are available from the corresponding author on reasonable request.

Electronic supplementary material

Supplementary information

Supplementary Files

This is a list of supplementary files associated with this preprint. Click to download.

- TABLE1.docx
- Supplementarytable1.docx
- Supplementaryinformation.docx
- WesternBlottingCCRCC2026.pdf
- FigureS1.tif